

Nuclear forward scattering and first-principles studies of the iron oxide phase Fe₄O₅

Karunakar Kothapalli,^{1,2,*} Eunja Kim,³ Tomasz Kolodziej,⁴ Philippe F. Weck,⁵ Ercan E. Alp,⁶ Yuming Xiao,⁷ Paul Chow,⁷ C. Kenney-Benson,⁷ Yue Meng,⁷ Sergey Tkachev,⁸ Andrzej Kozłowski,⁴ Barbara Lavina,^{1,3} and Yusheng Zhao^{1,3}

¹High Pressure Science and Engineering Center, University of Nevada, Las Vegas, Nevada 89154, USA

²Geophysical Laboratory, Carnegie Institution of Washington, Washington, DC 20015, USA

³Department of Physics and Astronomy, University of Nevada, Las Vegas, Nevada 89154, USA

⁴AGH University of Science and Technology, Kraków, Poland

⁵Sandia National Laboratories, Albuquerque, New Mexico 87185, USA

⁶Advanced Photon Source, Argonne National Laboratory, Argonne, Illinois 60439, USA

⁷High Pressure Collaborative Access Team, Geophysical Laboratory, Carnegie Institution of Washington, Argonne, Illinois 60439, USA

⁸GSECARS, University of Chicago, Building 434A, 9700 South Cass Avenue, Argonne, Illinois 60439, USA

(Received 3 November 2013; revised manuscript received 25 June 2014; published 29 July 2014)

⁵⁷Fe-enriched Fe₄O₅ samples were synthesized in a laser-heated diamond anvil cell at a pressure of about 15 GPa and a temperature of about 2000 K. Nuclear forward scattering (NFS) spectra were collected in the range 0–40 GPa and were combined with first-principles calculations to provide insights into the magnetic properties of Fe₄O₅. NFS spectra show that strong magnetic interactions persist up to 40 GPa and that they are generated by a single magnetic contribution. The hyperfine magnetic field (B_{hf}) and quadrupole splitting (QS) are in the ranges 51–53 T and 0.40–1.2 mm s⁻¹, respectively. The QS shows an intriguing evolution with pressure, with a fast increase from 0.4 to 1.0 mm s⁻¹ between 0 and 10 GPa and a slow increase up to 1.2 mm s⁻¹ in the range 10–40 GPa. First-principles calculations suggest an antiferromagnetic ordering for the three sites, and similar magnetic moments in the range ~ 3.6 – $3.8 \mu_{\text{B}}/\text{Fe}$. These values, typical of strongly correlated Fe magnetic systems, are in agreement with the experimental estimated average moment of $\sim 3.8 \mu_{\text{B}}/\text{Fe}$. The single contribution to the NFS spectrum and the similar calculated magnetic moments suggest that the iron atoms at the three crystallographic sites have similar electronic arrangements.

DOI: [10.1103/PhysRevB.90.024430](https://doi.org/10.1103/PhysRevB.90.024430)

PACS number(s): 62.50.-p, 75.47.Lx

I. INTRODUCTION

The compounds made of Earth's two most abundant elements are important in geology and biology. They have a wealth of industrial and technological applications [1] related to their unique physical properties. Fe₄O₅ was recently synthesized at about 10 GPa and 1800 K [2]. Fe₄O₅ is a mixed-valence oxide with an average iron formal charge of +2.5 and crystallizes in the orthorhombic *Cmcm* space group with ambient lattice parameters of $a = 2.8933 \text{ \AA}$, $b = 9.8092 \text{ \AA}$, and $c = 12.583 \text{ \AA}$. The structure may be viewed as FeO₆ edge-sharing octahedra arranged in layers stacked along the c axis alternating with face-sharing trigonal prisms (Fig. 1). It was later found that magnetite breaks down into Fe₄O₅ and hematite at pressures of over 9.5 GPa and over 1673 K [3], suggesting a fairly wide stability range of Fe₄O₅ at high pressure and temperature (PT). Fe₄O₅ is therefore very likely to occur in planetary interiors and therefore is of major petrological and geophysical significance. Iron oxides show an extraordinarily complex physics, and their electronic structures are strongly influenced by environmental conditions. The behavior of iron oxides is a prototype for several strongly correlated electron systems; the Verwey transition in magnetite discovered in 1939 [4] associated with a complex structural arrangement [5] is a classic example. Thus the discovery of an iron oxide renders the exploration of its properties imperative. This contribution reports an experimental investigation of the magnetic structure of Fe₄O₅. First-principles predictions of

the magnetic structure were also performed beyond standard density functional theory and used to provide guidance in interpreting experimental results.

Nuclear forward scattering (NFS) [6], also termed synchrotron Mössbauer spectroscopy (SMS), and its “incoherent analog” Mössbauer spectroscopy (MS) provide information about the oxidation state of the resonant isotope, its coordination number, spin state, and magnetic structure. It is an invaluable tool for studying iron oxides [7], particularly under pressure. The main advantage of NFS over conventional Mössbauer spectroscopy is that the source of incident photon or γ rays is a synchrotron. NFS is a readily accessible tool and ideal for high-pressure Mössbauer studies. The technique is particularly suitable for ⁵⁷Fe-enriched Fe₄O₅, which can only be synthesized in small amounts.

II. EXPERIMENT

Fe₄O₅ samples were synthesized from mixtures of Fe and ⁵⁷Fe-enriched Fe₂O₃ under pressure of 11–15 GPa and at temperatures around 2000 K. High-PT conditions were obtained using double-sided laser-heated (LH) diamond anvil cells (DACs) [8]. Brilliant and conical diamond anvils with 300- and 600- μm culet sizes were used for different samples and target pressures.

Rhenium gaskets with thickness of 250 μm were preindented to a thickness of 35–70 μm ; holes of 100–300 μm , depending on the culet size, were drilled to serve as sample chambers. Ruby spheres placed at the edge of the sample chamber were used to determine the pressure [9]. Neon, loaded at 1.7 kbar [10], was chosen as a pressure transmitting medium to ensure quasihydrostatic conditions.

*Corresponding author: kkothpalli@carnegiescience.edu

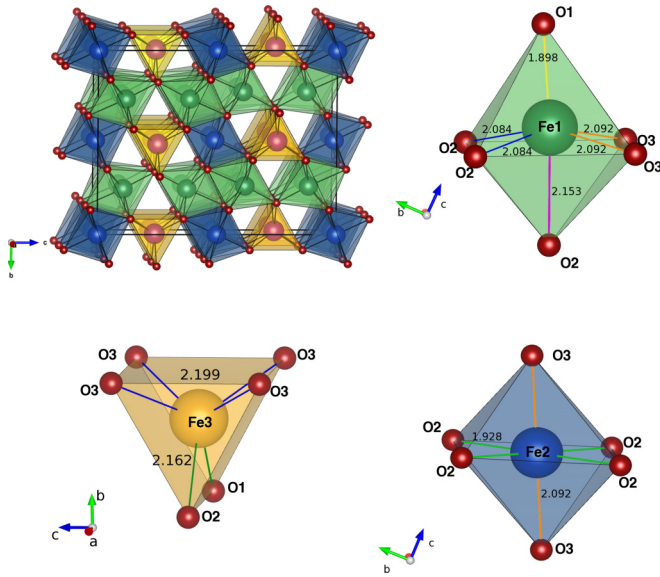


FIG. 1. (Color online) Crystal structure of Fe_4O_5 and iron first-coordination polyhedra. The green and blue octahedra show the local coordination of sites Fe1 (Wyckoff position $8f$) and Fe ($4a$) and the yellow trigonal prism shows the local environment at the Fe3 ($4c$) site. Ambient condition bond lengths, color coded for equivalence, emphasize the distortion of the polyhedra.

After synthesis, the sample composition and homogeneity were determined from x-ray diffraction pattern maps collected using highly focused x-ray beam [$4 \times 4 \mu\text{m}$ full width at half maximum (FWHM), 29 keV] and MARCCD detector at the experimental station 16ID-B, at HPCAT, Advanced Photon Source, Argonne National Laboratory (APS, ANL). Owing to the large thermal gradients across the sample, typical of the LHDAC technique, the high-PT synthesis did not produce perfectly homogeneous Fe_4O_5 samples. In some of the syntheses, diffraction patterns confirmed the presence of unreacted hematite and wüstite in addition to Fe_4O_5 . Our diffraction maps showed that hematite is mostly confined at the sample rims while FeO is confined to a minor region of the sample. The Fe_4O_5 yield of the samples used in our spectroscopic experiments is $\sim 85\%$. Rough estimation of phase abundances in each spot were determined using the MDI JADE 5.0 software (Materials Data Inc., Liverpool, CA).

NFS spectra were collected at the Advanced Photon Source, Argonne National Laboratory, on sample regions consisting of nearly pure Fe_4O_5 . Room temperature spectra in the range 11–41 GPa were collected at beamline 3ID-B, while the spectra in the range 0–32 were collected at beamline 16ID-D. The incident beam of high-flux x rays with a resolution of 1 meV at 3ID-B and 2 meV at 16ID-D was monochromated to the ^{57}Fe nuclear resonance energy of ~ 14.4125 keV. The beam FWHM at 3ID-B and 16ID-D was 10×10 and $30 \times 50 \mu\text{m}$, respectively. The beam spot at 16ID-D was further reduced using a $20\text{-}\mu\text{m}$ pinhole for later runs to reproduce the results. The intensities of the resonantly scattered photons in the forward direction with 153.4 ns separation between the individual bunches were recorded by an avalanche photodiode detector. Spectra at each pressure were collected for about 2 h. The program CONUSS [11] was

used to analyze the spectra and to determine the hyperfine field (B_{hf}) and quadrupole splitting (QS) parameters.

III. RESULTS AND DISCUSSIONS

A. Interpretation of NFS spectra

The rich quantum beat patterns shown in Fig. 2 reveal strong magnetic interactions in Fe_4O_5 persisting in the investigated pressure range. The Mössbauer effect generates a subspectrum from each magnetic sublattice, a sextet in the case of conventional Mössbauer spectra. Thus we expected to discriminate at least two distinct magnetic sublattices in Fe_4O_5 as iron atoms are arranged in three nonequivalent crystallographic sites. Several models were tested against the data; it quickly appeared that a single magnetic contribution explains most of the spectra features. We nonetheless fitted our data with both a two-magnetic-sites model (“2-site”) and a single-magnetic-site model (“1-site”). In the first case, we constrained the sum of their weights to unity so that their combined contribution adds up to 100%. At ambient pressure, the 2-site model yielded a dominant site with a contribution of about 93.5% and $B_{\text{hf}} \sim 52.11$ T and a second site with a small contribution of about 6.5% and $B_{\text{hf}} \sim 6$ T.

The contribution from the second site diminished substantially with increasing pressure and at 41 GPa it is reduced to less than 2%. The decrease was greatest in the pressure range 0–11 GPa going from 6.5% to 3.5%. The 1-site model produced parameters for the unique site that are the same, within uncertainties, as those of the dominant site for the

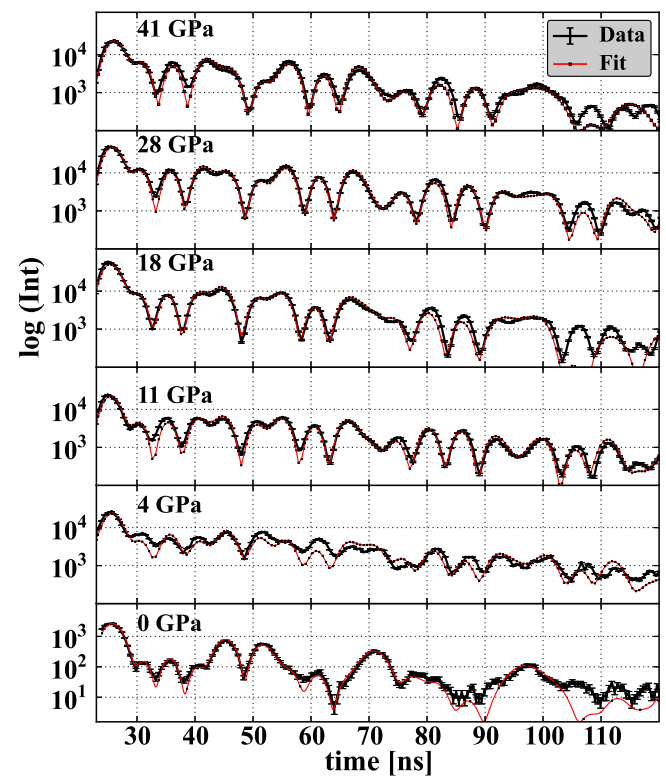


FIG. 2. (Color online) Representative NFS spectra (black) and fits to the spectra (red online), based on the 1-site model at different pressures in the range 0–41 GPa at room temperature.

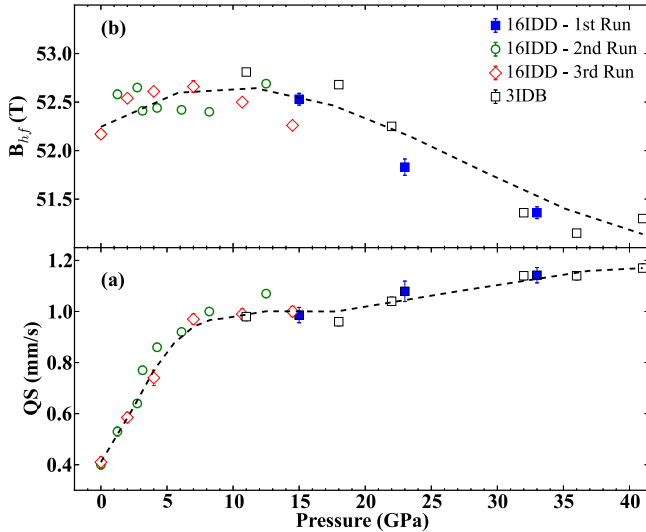


FIG. 3. (Color online) Pressure dependencies of (a) quadrupole splitting (QS); (b) hyperfine magnetic field (B_{hf}) derived from fitting the NFS spectra with a 1-site model. The consistency and overlap of different symbols representing data collected on different samples at different beamlines show the sample and resolution independence of the hyperfine parameters. Error bars, wherever not visible, are smaller than the size of the symbol.

2-site model. Fitting statistics are essentially the same in the two cases; within the resolution of our experiment we are therefore able to discuss the behavior of one undistinguished magnetic sublattice only; the presence of a second, minor but distinct magnetic site is dubious. It follows that in Fe_4O_5 either one or more iron atoms are nonmagnetic, a scenario proposed for $h\text{-Fe}_3\text{O}_4$ [12], or that the three sites generate overlapping subspectra. Based on our first-principles results (see below) we find that the second hypothesis is more likely.

The fits to the spectra are very satisfactory at all pressures. The pressure dependence of the QS and the B_{hf} up to 41 GPa obtained with the 1-site model are shown in Fig. 3. Measurements performed on different samples and beamlines are in excellent agreement, suggesting that minor impurities do not hinder the determination of Fe_4O_5 hyperfine parameters.

B. Quadrupole splitting and hyperfine magnetic field

The QS of Fe_4O_5 at ambient conditions is 0.4 mm s^{-1} ; its pressure dependence, shown in Fig. 3(a), shows a two-stage behavior. The QS increases at a rate of about $0.1 \text{ mm s}^{-1}/\text{GPa}$ up to roughly 10 GPa, and then slowly increases up to 1.2 mm s^{-1} at 40 GPa. The QS values fall in the range typical of Fe^{3+} ions with six oxygen ligands in the high-spin state [13,14], approximately between 0 and 1.2 mm s^{-1} . The QS of most six-coordinate Fe^{2+} in high-spin state is typically in the range $2.0\text{--}3.6 \text{ mm s}^{-1}$; we can therefore exclude that our magnetic sublattice(s) is generated by HS- Fe^{2+} . B_{hf} values (see below) also support this interpretation. The average formal iron valence state in the investigated compound is $2.5+$; we therefore expected to observe distinct Fe^{2+} and Fe^{3+} sublattice spectra. A possible explanation of our observations, strongly supported by our theoretical predictions, is that the average

charge of our sites is noninteger and similar in the three sites. Indeed, the trend of increase in QS, from ~ 0.40 to $\sim 1.2 \text{ mm s}^{-1}$ between 0 and 40 GPa, is remarkably similar to that of Fe^{3+} ions in the six-coordinated octahedral position in Fe_3O_4 [15] albeit the magnitudes of Fe_4O_5 are much larger. A comparison of relative magnitudes and the pattern of pressure dependence of QS and also B_{hf} strongly suggests a noninteger valence state in Fe_4O_5 [13–17], a value lower compared to that in magnetite but higher than Fe^{2+} . Because the FeO_6 octahedra share edges, it is plausible that electron transfer occurs between the iron atoms occupying the two octahedral sites. At ambient conditions, the distances between iron pairs $4a\text{-}8f$, $4a\text{-}4c$, and $8f\text{-}4c$ are 2.893, 3.385, and 2.898 Å, respectively. These distances compare very favorably with the distance between the octahedral iron atoms in magnetite (2.97 Å) among which electron transfer occurs. Electron transfer between octahedral iron atoms has been documented for CaFe_3O_5 [18], which is isostructural with Fe_4O_5 .

In Fe_4O_5 , short Fe-Fe distances occur also between the trigonal prism and the octahedral $8f$ sites; hence it is plausible that the charge transfer involves the trigonal prism site as well. In a scenario where multiple charge transfer channels with different probabilities exist, dynamic transfer, as in magnetite above the Verwey temperature, or a complex quasi-static-charge order state, such as the trimeron lattice in magnetite at low temperature [5], may occur, resulting in mixed time-averaged valences in all sites. Such a noninteger charge dynamic or static state can also be supported by the existing literature data; indeed, the values of QS in the range $0\text{--}1.2 \text{ mm s}^{-1}$, as found by our team, are reported [19,20]. Both the experimentally obtained magnetic moment values and those calculated (see below) suggest that the charge order in Fe_4O_5 may resemble that of magnetite in the octahedral sites.

The hyperfine magnetic field, B_{hf} , has magnitude and pressure dependence typical of Fe^{3+} ions in high-spin state in sixfold coordination in agreement with the values of QS [13,14]. The B_{hf} increases at first and plateaus around 10 GPa and then gradually decreases. Again, this pressure dependence of B_{hf} is remarkably similar to the behavior of $\text{Fe}^{2.5+}$ ions in octahedral sites [17] indicating the noninteger valency. An approximate estimation of the magnetic moment can be obtained by simply dividing the measured value of B_{hf} by $\sim 15 \text{ T}/\mu_{\text{B}}$; which is in turn obtained by dividing the value of B_{hf} measured for a metallic Fe (33.9 T at 4 K) by the value of the magnetic moment per Fe atom in iron ($2.2 \mu_{\text{B}}$) [21]. We obtained a magnetic moment $\sim 3.5 \mu_{\text{B}}/\text{Fe}$ —very typical of correlated Fe magnetic systems. The covalency of bonding electrons increases as the pressure increases and hence the decrease in magnetic moment.

C. Computational results on the magnetic properties of Fe_4O_5

In order to gain insights into the magnetic properties of this material, first-principles total-energy calculations were performed using the spin-polarized density functional theory (DFT) as implemented in the Vienna *ab initio* simulation package (VASP) [22]. The exchange-correlation energy was calculated using the generalized gradient approximation (GGA) with the parametrization of Perdew and Wang (PW91) [23].

The interaction between valence electrons and ionic cores was described by the projector augmented wave (PAW) method [24,25]. The Fe ($3d^6, 4s^2$) and O ($2s^2, 2p^4$) electrons were treated explicitly as valence electrons in the Kohn-Sham (KS) equation and the remaining core electrons together with the nuclei were represented by PAW pseudopotentials. The plane-wave cutoff energy for the electronic wave functions was set to a value of 500 eV, ensuring the total energy of the system to be converged to within 2×10^{-6} eV/atom. A periodic unit cell containing four formula units was used in the calculations, i.e., 36 atoms (16 Fe and 20 O atoms) were included in the Fe_4O_5 unit cell. Electronic relaxation was performed with the conjugate gradient method accelerated using the Methfessel-Paxton Fermi-level smearing [26]. Ionic relaxation was carried out using the quasi-Newton method and the Hellmann-Feynman forces acting on atoms were calculated with a convergence tolerance set to 0.001 eV/Å. The Brillouin zone was sampled using the Monkhorst-Pack special k -point scheme [27] with a $3 \times 3 \times 3$ mesh for structural optimization and total-energy calculations. In order to accurately describe iron oxide systems with localized Fe $3d$ electrons, the GGA+ U method was introduced in the total-energy calculations [28].

The total-energy curves for the various combinations of spin alignments of Fe atoms at $4a$, $8f$, and $4c$ positions are calculated using DFT, as shown in Fig. 4. Refined total-energy calculations indicate that the ground state of Fe_4O_5 is antiferromagnetic (AFM) ($- + -$), while the ferromagnetic state (FM) ($+ + +$) is the least favorable. The pressure dependency of the magnetic moments was examined for the antiferromagnetic ground state of Fe_4O_5 , as depicted in Figs. 5(a)–5(c). The AFM structure comprises two magnetic sublattices, i.e., one formed by Fe atoms occupying the $8f$ sites and the other equal and oppositely directed magnetic sublattices formed by atoms occupying the $4a$ and $4c$ sites. The energy difference between AFM and the second most energetically favorable ferrimagnetic (FRM) are relatively small (less than about

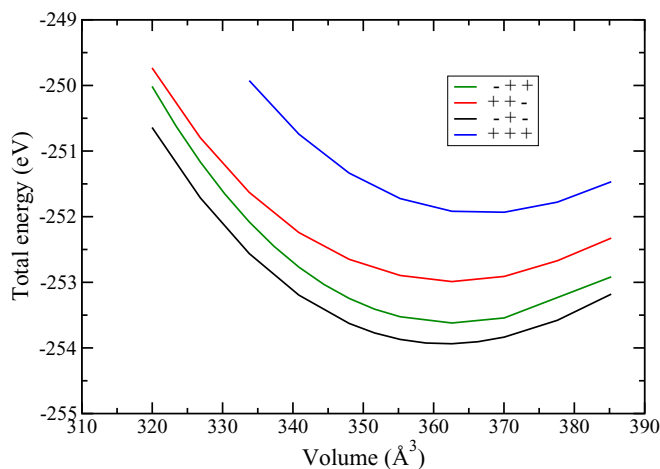


FIG. 4. (Color online) Total-energy curves for different spin arrangements from first-principles calculations. The + and – notations represent the spins up and down, respectively at $4a$, $8f$, and $4c$ sites. (++++) corresponds to a ferromagnetic (FM) state, (– + –) and (– + –) correspond to ferrimagnetic (FRM) states and (– + –) corresponds to an antiferromagnetic (AFM) state.

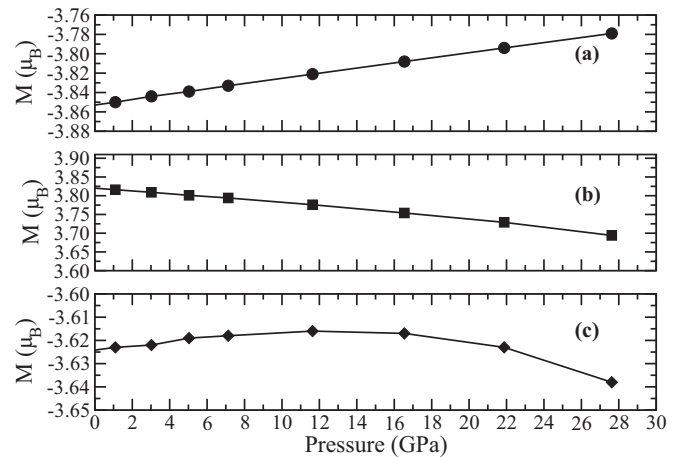


FIG. 5. Calculated pressure dependencies of magnetic moment at $4a$, $8f$, and $4c$ and sites in panels (a)–(c) respectively.

0.2 eV per formula units), suggesting that temperature- and/or pressure-driven spin transitions are plausible. The pressure-induced decrease in magnetic moments of the two octahedral iron atoms is similar and is comparable to that observed by Klotz [29] in magnetite.

The magnitude of the magnetic moments of the Fe atoms is similar for all sites and far from the values predicted by Fe^{3+} and Fe^{2+} ionic models. The moments at $4a$ and $8f$ sites decrease linearly with pressure as seen in Figs. 5(a) and 5(b). However, the magnetic moment at the $4c$ site is rather intriguing, with a monotonic decrease with pressure up to 12 GPa followed by an increase above 16 GPa, as shown in Fig. 5(c); this suggests a possible change in the bonding environment of the Fe atoms at the $4c$ site with pressure. Such a change in bonding environment would be consistent with the pressure dependence of the QS. Our DFT finding indicates that at the $4c$ site all the bond lengths of Fe-O at 21.9 GPa become 2.01 Å, while there are two of 2.02 Å and four of 2.12 Å at 16.5 GPa in the isosceles-triangular prism.

The three crystallographic iron sites have similar magnetic moments and, considering that the effects of atoms in the second coordination are very subtle, this collinear AFM structure produces almost overlapping subspectra which could not be resolved in our NFS experiment. Therefore, we can conclude that our experimental one-site dominant line spectrum is in a reasonable agreement with the theoretical predictions and that further experimental evidence is essential to resolve all the magnetic sublattices.

IV. CONCLUSIONS

Our combined experimental and theoretical results suggest that the three iron sites of Fe_4O_5 have similar configuration. In particular, we found that NFS spectra are generated by a single indistinguishable component with a mean magnetic moment $3.8 \mu_B/\text{Fe}$ site estimated from the hyperfine field. Also, first-principles calculations show that the three sites have a similar magnetic moment (3.6, 3.8, $3.8 \mu_B$ for the three crystallographic Fe sites). The QS and B_{hf} values of the Fe_4O_5 magnetic site are comparable with the values observed for octahedral sites of magnetite [17] where noninteger charge density

distribution occurs. We therefore suggest that the uniformity of Fe magnetic sites in Fe_4O_5 is due to a noninteger valence arrangement, possibly including orbital ordering. Our results do not allow us to determine whether the proposed arrangement is static, as in low-temperature magnetite, or dynamic. Further investigations, including pressure- and temperature-dependent diffraction and magnetic and spectroscopic measurements, are required in order to unambiguously resolve the charge on each site and the details of the magnetic structure.

ACKNOWLEDGMENTS

This research was sponsored in part by High Pressure Science and Engineering Center (HiPSEC: a DOE/NNSA Center of Excellence) through DOE Cooperative Agreement

No. DE-NA0001982. E.K. acknowledges funding through a subcontract with Los Alamos National Laboratory within the Department of Energy's Fuel Cycle R&D program. Sandia National Laboratories is a multiprogram laboratory managed and operated by Sandia Corporation, a wholly owned subsidiary of Lockheed Martin Corporation, for the U.S. Department of Energy's National Nuclear Security Administration under Contract No. DE-AC04-94AL85000. Portions of this work were performed at HPCAT (Sector 16), Advanced Photon Source (APS), Argonne National Laboratory. HPCAT operations are supported by DOE-NNSA under Award No. DE-NA0001974 and by DOE-BES under Award No. DE-FG02-99ER45775, with partial instrumentation funding by NSF. APS is supported by DOE-BES, under Contract No. DE-AC02-06CH11357.

-
- [1] R. M. Cornell and U. Schwertmann, *The Iron Oxides: Structure, Properties, Reactions, Occurrences and Uses*, 2nd ed. (Wiley-VCH Verlag GmbH & Co. KGaA, Weinheim, 2004).
- [2] B. Lavina, P. Dera, E. Kim, Y. Meng, R. T. Downs, P. F. Weck, S. R. Sutton, and Y. Zhao, *Proc. Natl. Acad. Sci. USA* **108**, 17281 (2011).
- [3] A. B. Woodland, D. J. Frost, D. M. Trots, K. Klimm, and M. Mezouar, *Am. Mineral.* **97**, 1808 (2012).
- [4] E. J. W. Verwey, *Nature* **144**, 327 (1939).
- [5] M. S. Senn, J. P. Wright, and J. P. Attfield, *Nature* **481**, 173 (2012).
- [6] R. Röhlberger, *Nuclear Condensed Matter Physics with Synchrotron Radiation: Basic Principles, Methodology and Applications* (Springer, Berlin, 2004).
- [7] G. Calas and F. Hawthorne, *Rev. Mineral.* **18**, 1 (1988).
- [8] W. A. Bassett, *Rev. Sci. Instrum.* **72**, 1270 (2001).
- [9] H. K. Mao, J. Xu, and P. M. Bell, *J. Geophys. Res. Solid Earth* **91**, 4673 (1986).
- [10] M. Rivers, V. B. Prakapenka, A. Kubo, C. Pullins, C. M. Holl, and S. D. Jacobsen, *High Press. Res.* **28**, 273 (2008).
- [11] W. Sturhahn, *Hyperfine Interact.* **125**, 149 (2000).
- [12] W. M. Xu, G. Y. Machavariani, G. K. Rozenberg, and M. P. Pasternak, *Phys. Rev. B* **70**, 174106 (2004).
- [13] G. Bancroft, A. Maddock, and R. Burns, *Geochim. Cosmochim. Acta* **31**, 2219 (1967).
- [14] *Spectroscopic Methods in Mineralogy and Geology*, edited by F. C. Hawthorne, Reviews in Mineralogy Vol. 18 (Mineralogical Society of America, Washington, DC, 1988).
- [15] H. Kobayashi, I. Isogai, T. Kamimura, N. Hamada, H. Onodera, S. Todo, and N. Mori, *Phys. Rev. B* **73**, 104110 (2006).
- [16] G. K. Wertheim, *Mössbauer Effect: Principles and Applications* (Academic Press, New York, 1964).
- [17] K. Glazyrin, C. McCammon, L. Dubrovinsky, M. Merlini, K. Schollenbruch, A. Woodland, and M. Hanfland, *Am. Mineral.* **97**, 128 (2012).
- [18] R. Gerardin, E. Millon, J. Brice, O. Evrard, and G. Lecaer, *J. Phys. Chem. Solids* **46**, 1163 (1985).
- [19] J. Zukrowski (private communication).
- [20] F. J. Berry, S. Skinner, and M. F. Thomas, *J. Phys.: Condens. Matter* **10**, 215 (1998).
- [21] S. M. Dubiel, *J. Alloys Compd.* **488**, 18 (2009).
- [22] G. Kresse and J. Furthmüller, *Phys. Rev. B* **54**, 11169 (1996).
- [23] J. P. Perdew and Y. Wang, *Phys. Rev. B* **45**, 13244 (1992).
- [24] P. E. Blöchl, *Phys. Rev. B* **50**, 17953 (1994).
- [25] G. Kresse and D. Joubert, *Phys. Rev. B* **59**, 1758 (1999).
- [26] M. Methfessel and A. T. Paxton, *Phys. Rev. B* **40**, 3616 (1989).
- [27] H. J. Monkhorst and J. D. Pack, *Phys. Rev. B* **13**, 5188 (1976).
- [28] S. L. Dudarev, G. A. Botton, S. Y. Savrasov, C. J. Humphreys, and A. P. Sutton, *Phys. Rev. B* **57**, 1505 (1998).
- [29] S. Klotz, G. Steinle-Neumann, T. Strässle, J. Philippe, T. Hansen, and M. J. Wenzel, *Phys. Rev. B* **77**, 012411 (2008).